Metal to insulator transition in Sb doped SnO_2 monocrystalline nanowires thin films

I. M. Costa, E. P. Bernardo, B. S. Marangoni, E. R. Leite, and A. J. Chiquito

Citation: Journal of Applied Physics **120**, 225109 (2016); doi: 10.1063/1.4971870
View online: https://doi.org/10.1063/1.4971870
View Table of Contents: http://aip.scitation.org/toc/jap/120/22
Published by the American Institute of Physics

Metal to insulator transition in Sb doped SnO_2 monocrystalline nanowires thin films

I. M. Costa,[1] E. P. Bernardo,[1] B. S. Marangoni,[2] E. R. Leite,[3] and A. J. Chiquito[1]
[1]*NanO LaB—Departamento de Física, Universidade Federal de São Carlos, CEP 13565-905, CP 676 São Carlos, São Paulo, Brasil*
[2]*Instituto de Física, Universidade Federal do Mato Grosso do Sul, P.O. Box 549, CEP 79070-900 Campo Grande, MS, Brasil*
[3]*LIEC—Departamento de Química, Universidade Federal de São Carlos, CEP 13565-905, CP 676 São Carlos, São Paulo, Brasil*

(Received 7 July 2016; accepted 24 November 2016; published online 15 December 2016)

We report on the growth and transport properties of single crystalline Sb doped SnO_2 wires grown from chemical vapour deposition. While undoped samples presented semiconducting behaviour, doped ones clearly undergo a transition from an insulating state ($dR/dT < 0$) to a metallic one ($dR/dT > 0$) around $130-150\ K$ depending on the doping level. Data analysis in the framework of the metal-to-insulator transition theories allowed us to investigate the underlying physics: electron-electron and electron-phonon interactions were identified as the scattering mechanisms present in the metallic phase, while the conduction mechanism of the semiconducting phase (undoped sample) was characterized by thermal activation and variable range hopping mechanisms. *Published by AIP Publishing*. [http://dx.doi.org/10.1063/1.4971870]

I. INTRODUCTION

Transparent conducting oxides are largely used in different optoelectronic applications. Usually, Indium Tin oxide (ITO) is frequently chosen because of its high transmittance in the visible region and low resistivity. However, because of the high cost of metallic indium there is an intense search for proper substitutes. Among them, the wide band gap SnO_2 (3.6–4.0 eV)[1,2] is an alternative. SnO_2 is an intrinsic n-type semiconductor (mostly induced by oxygen vacancies) usually found in a rutile structure.[3] As observed in ITO, the coexistence of low resistivity and optical transparency is a characteristic feature of this class of materials. In fact, this feature makes SnO_2 an excellent material for gas sensing devices either as thin films or as nanowires and nanobelts.[4]

The primary source of carriers is ionized (fully or partially) oxygen vacancies which act as shallow donors. Unfortunately, they cannot be easily controlled in order to produce a reliable device. As in other semiconductor materials, precise control of electrical properties of SnO_2 is achieved by doping processes using different impurities such as In, Sb, Pd, Al, Pt, Cu, Zn, Mn, and F.[5–14] As a result, the control of conductivity was readily observed in these papers as expected.

Antimony is one of the most used doping materials due to its facility of incorporation in the SnO_2 lattice leading to measurable improvements in electrical conductivity and optical transparency.[3,15] White *et al.*[16] have conducted a well controlled study of Sb doped SnO_2 (ATO) thin films over a range of electron concentrations showing that there were no deleterious effects to the crystalline quality due to Sb incorporation. Usually, Sb doping gives rise to an impurity semi-occupied band below the conduction band bottom of the oxide, controlling the conduction properties of the SnO_2.[17] Also, Sb doped SnO_2 (ATO) nanowires show a faster recovery time than that measured in pure SnO_2 nanowires demonstrating their potential photon-sensing application.[18] In some experiments, ATO nanowires exhibit resistivities as low as observed in metallic conductors ($4.09 \times 10^{-4}\Omega\,\mathrm{cm}$).[19]

As recently observed by Li *et al.* using theoretical calculations, pure (undoped) SnO_2 showed a semiconductor electronic structure, but a metal-like band structure is observed when Sn atoms were replaced by Sb atoms (corresponding to 6.25% doping level). They observed that the presence of oxygen vacancies in Sb doped SnO_2 increases the density of states at the Fermi level, resulting in a consequent increase of the conductivity. The metal-like structure certainly affects the conductivity of the doped system. In fact, the authors obtained a very high carrier concentration from their calculations ($1.78 \times 10^{21}\mathrm{cm}^{-3}$).[20] This high electron density is large enough to allow a semiconductor-to-metal transition guided by the Mott criterion $n_c^{1/3} a_B = 0.26$, where n_c is the critical density and a_B is the Bohr radius (for SnO_2, $n_c = 6.7 \times 10^{17}\mathrm{cm}^{-3}$). Chang *et al.*[21] reported a metal-insulator transition in ATO thin films as a function of film thickness for a fixed Sb doping level proposing a generalized energy diagram to describe the thickness induced transition. Also recently, Serin *et al.*[22] observed a doping-induced MIT in ATO thin films prepared by a sol-gel route driven by electron-electron interactions (EEI).

However, impurity doping provides either free carriers or some degree of disorder which is added to the intrinsic disorder of the material. In a certain degree of disorder, the system experiences a transition from a metallic to an insulator (or semiconducting) state when carriers, at the Fermi level, become localized. Such a transition is referred to as Anderson transition: carriers subjected to a random electrostatic potential are not able to move freely through the system if either potential fluctuations due to disorder exceed a critical value or the electron energy is lower than the characteristic potential fluctuation. In this limit, the metallic conduction is

then replaced by an insulating regime where the system is characterized by strong localization of carriers.[23] In that degenerated system electron–electron interactions (EEI) result in quantum corrections to the classical Boltzmann conductivity on the metallic phase and when a material shows a phase–breaking length larger than the localization length (in the limit of weak disorder $k_F l > 1$) the system is said to be in the weakly localized regime.[24]

In this paper, we studied single crystalline Sb doped SnO_2 wires grown from chemical vapour deposition. The incorporation of Sb atoms into the SnO_2 lattice increases the doping level leading to a clear transition from a semiconductor to a metallic behaviour; a reasonable correspondence between the resistivity and the incorporated dopant concentration was also observed. In order to explore microscopic mechanisms leading to the observed transport characteristics, we have recorded the temperature dependent resistivity of several samples with distinct doping levels. Data analysis in the framework of the metal-to-insulator transition theories allowed us to investigate the underlying physics: electron-electron interactions were identified as the scattering mechanisms present in the metallic phase while the conduction mechanism of the semiconducting (insulating undoped sample) phase was characterized by thermal activation and variable range hopping mechanisms.

II. EXPERIMENTAL

ATO samples were synthesized by thermal evaporation of a mixture of Sn/Sb metal powders under the usual vapour-liquid-solid mechanism procedures. High purity Sn and Sb (Aldrich, 99.99%) powders were mixed at different proportions by using a ball mill for 24 h. The doping level was defined from the Sb/(Sn+Sb) ratio for each sample. The powder mixture and Au coated SiO_2/Si substrates (2 nm) were put in an alumina crucible (8 cm long) and then placed at the center of a horizontal tube furnace (Lindberg Blue M) where temperature, pressure, and evaporation time were controlled in order to obtain the optimal conditions for the synthesis. The powder precursors and coated substrates were separated by 5 cm (downstream) in the alumina crucible. The pressure inside the tube was controlled by a vacuum pump around 200 mbar and an Argon/Oxygen mixture with a constant flow of 100/5 sccm was used for the vapour transport to the synthesis region. The furnace was heated up to 950 °C in 50 min and the temperature was held at 950 °C during the whole synthesis process (90 min). Then, the furnace was left to cool down to the room temperature naturally. After the cooling time, the substrates were covered by a blue-white film of nanowires (40–100 nm wide and tens of microns long) and microwires (100 nm–4 μm wide and hundreds of microns long) as observed in Fig. 1(a). The structure was analysed by X-ray diffraction (Shimadzu, XRD 6100, 40 kV, 30 mA, Cu K α radiation).

For transport studies, devices were built from a large dispersion of nanowires ($\sim 10^5$ wires/cm^2) and hereafter referred to as thin film samples. Studying a dispersion of nanowires/microwires we obtain parameters that statistically represent the mean response of the system avoiding errors when choosing a

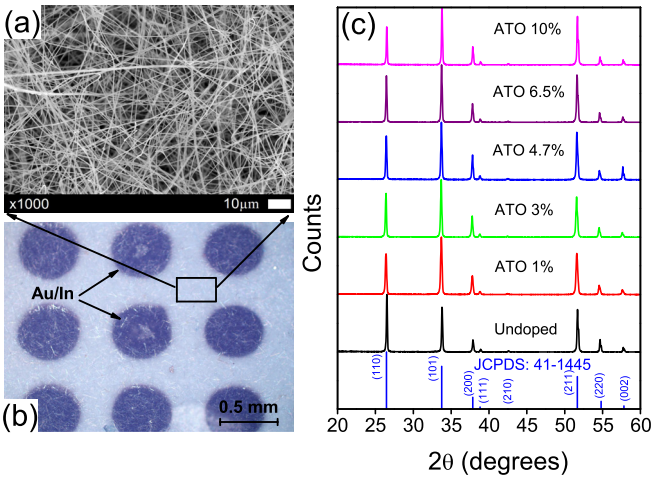

FIG. 1. Panel (a) shows a scanning electron microscopy image of the as-grown samples. An optical image of a nanowire thin film device with metal electrodes (Au/In, 80/20 nm) of 0.5 mm in diameter and separated by 0.3 mm is shown in panel (b). X-ray diffraction patterns of as-grown samples are shown in panel (c). All diffraction peaks were indexed as the tetragonal structure of SnO_2 within the P42/mnm spatial group and there is no additional phase peak in the X-ray diffraction pattern even for the highest Sb doping level. No significant changes of the lattice parameters were found.

particular wire. Also, being single-crystalline structures and having dimensions which are comparable in thickness with most ATO thin films studied in the literature (but always having polycrystalline structures), we are able to compare our results with them. The devices in Fig. 1(b) were produced as following: as-grown wires were ultrasonically dispersed in ethanol and were placed on SiO_2 (500 nm thick) covered Silicon substrates; then, metal electrodes (0.5 mm diameter and separated by 0.3 mm) were micro-fabricated using standard lithographic/masking techniques (Au/In, 80/20 nm). Then, substrates were treated at 350 °C for 10 min in a tube furnace filled with an inert atmosphere of Argon.

Four probe transport measurements were carried out at different temperatures from 10 to 300 K using a closed-cycle helium cryostat (Janis model CCS150). The samples were kept at a pressure lower than 5×10^{-6} mbar. The resistance was obtained using standard low frequency ac lock-in (Signal Recovery model 7265) at $f = 13$ Hz and dc techniques (Keithley SMU model 2400C), but the results were unchanged. We used different current levels in the experiments in order to avoid non-linear transport due to high field effects and undesired Joule heating. Initial electrical characterization (current-voltage curves) showed a linear shape and as expected. We also conducted four and two probe measurements in different samples, but the resistivity/resistance remained unchanged in the whole temperature range used. Conventional van der Pauw[25] Hall measurements were conducted at room temperature and at B = 1 T using lock-in detection (LakeShore Cryogenics, model EM7 magnet).

III. STRUCTURAL AND DOPING ANALYSES

The XRD patterns for all samples are shown in Fig. 1(c). All diffraction peaks were indexed as the tetragonal structure of SnO_2 within the P42/mnm spatial group (JCPDS card number 41–1445) and there is no additional phase peak

in the XRD pattern even for the highest Sb doping level. The intensity ratio between reflections [110] and [101] for the undoped sample gives an indication of a preferential orientation growth, when compared with the standard data ($I_{(110)}/I_{(101)} = 1.33$), due to the large aspect ratio of the morphology of those samples. In addition to this morphological effect, as the doping level increases the intensity of [101] family reflection increases indicating that the Sb doping affects the preferential growth. Similar behaviour was observed in ATO thin films and it was attributed to the incorporation of Sb in the structure.[26] Additionally, XRD patterns were analysed in the Rietveld refinement method framework[27,28] using the GSAS package.[29,30] The extracted parameters are shown in Table I. We do not find significant changes in the lattice parameters as a function of the increasing doping level. The Sb doping seems not to strongly affect the structure of the SnO_2 for the undoped sample $a = b = 4.7399(1)$ Å e $c = 3.1881(1)$ Å, while for the highest doped sample $a = b = 4.7411(1)$ Å e $c = 3.1887(1)$ Å. These findings are in agreement with the literature: antimony can be incorporated in the SnO_2 lattice as pentavalent (Sb^{5+}, acting as a donor) or trivalent (Sb^{+3}, acting as an acceptor) ions. Sb^{5+} ions have an ionic radius smaller (0.6 Å) than that of Sn^{4+} (0.69 Å) and no significant distortion of SnO_2 lattice is observed.[16,31–34]

In order to study the incorporation of Sb atoms in our samples, the Laser Induced Breakdown Spectroscopy (LIBS) technique was used. The experiment was performed by a benchtop double pulse LIBS with an intensified CCD acquisition system. The lasers were arranged in collinear geometry. The first shot laser was a 532 nm and the second (reheating shot) was a 1064 nm. The 532 nm laser was generated by a Nd:YAG Q-Switch laser (Quantel) with a maximum energy of 180 mJ and 4 ns width and the 1064 nm laser was generated by a Nd:YAG Q-Switch laser (Quantel) with a maximum energy of 75 mJ and 6 ns width per pulse. The plasma light was collected by an optic fiber located 5 cm far from sample and delivered to a spectrometer (400-Butterfly Ariele, Andor) operating in a range of 175–330 nm with a spectral resolution of 13–24 pm. The spectra were recorded by an ICCD camera (1024 × 1024 pixels). The interpulse delay was set in 500 ns with a 10 μs integration gate. A delay generator (Quantum Composers) was used to synchronize the laser shots and acquisition. All measurements were carried in atmospheric air at ambient pressure without any sample preparation. The measurements were performed *in situ* in the same substrate where nanowires were grown. Fifteen spectra were acquired from each sample at different positions. Each spectrum was the result of two accumulated laser pulse. A routine based on spectral angle distance[35,36] was used to automatically exclude outliers spectra. The total number of excluded spectra was less than 3% of total set. The remaining spectra were averaged resulting in one final spectrum per sample.

TABLE I. Lattice parameters for undoped and Sb doped SnO_2 obtained from Rietveld refinement.

Sample	$a = b$(Å)	c(Å)
Undoped SnO_2	4.7399(1)	3.1881(1)
SnO_2: 1%Sb	4.7418(1)	3.1891(1)
SnO_2: 3%Sb	4.7427(1)	3.1895(1)
SnO_2: 4.7%Sb	4.7417(1)	3.1894(1)
SnO_2: 6.5%Sb	4.7376(1)	3.1872(1)
SnO_2: 10%Sb	4.7411(1)	3.1887(1)

Fig. 2 shows the results of calibration free-LIBS (CF-LIBS) using Sb (1%) precursor sample as normalization. The curve clearly shows a linear trend indicating the aggregation of Sb in samples with the increase of precursor percentage. Because of the qualitative aspect of the measurement, the unitary proportion between precursor and aggregation was not respected. This result was expected and can be related to the necessity of a better normalization procedure and due to a lack of an experimental parameter calibration, a reference material to improve the model is necessary. The spectra were used in a crude form without any complex pretreatment or calibration; just a simple routine to remove outliers was implemented. The goal was to prove the increase of the Sb content in the samples as the precursor percentage increases. In order to improve this measurement, we propose an optimization on laser pulse delay and time acquisition and the use of certificate materials to calibrate the results. As far as we know, this is the first application of LIBS in doped SnO_2 samples. A more accurate study will be developed to refine this kind of measurement and a separate work will be devoted to that.

IV. TRANSPORT DATA

The data from LIBS were confirmed by Hall measurements. Fig. 2 depicts the Sb doping level as a function of Sb content. Comparing the LIBS profile and Hall data for all samples, there is strong evidence showing the increase of Sb incorporation in the SnO_2 matrix related to the precursor percentage. This result also agrees with the resistivity dependence on the Sb content in different samples as depicted in Fig. 3(a).

Before deeper investigations, we need to distinguish the contribution from vacancies and from doping to the measured transport parameters. This is necessary because SnO_2 is an intrinsic n-type semiconductor in which electrical properties are mostly induced by oxygen vacancies. In order to accomplish this task, we used a simple procedure: doped samples were thermally treated in an oxidizing atmosphere

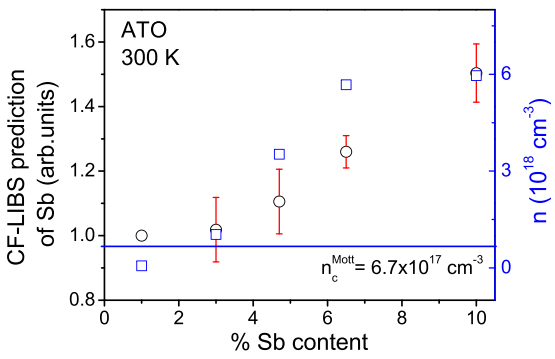

FIG. 2. Calibration free LIBS prediction for Sb doping ATO samples and the doping levels from Hall data are plotted.

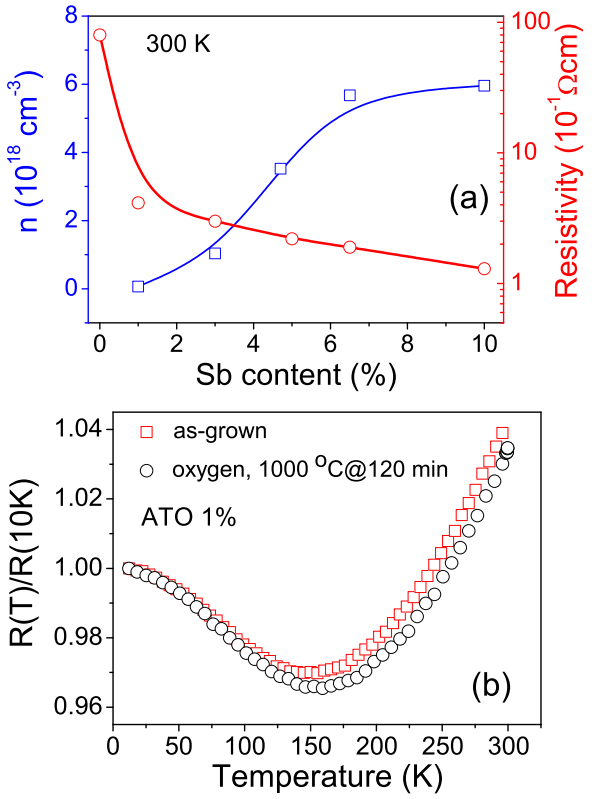

FIG. 3. Panel (a) depicts the resistivity and doping level dependence on the Sb content in different samples showing a reasonable agreement. Panel (b) shows the temperature dependent resistivity of a device before and after a thermal treatment at 1000 °C under an oxygen atmosphere. The resistance remains unchanged after the thermal treatment.

(O_2) for 120 min at 1000 °C and the resistivity was measured before and after the treatment. If Sb atoms were not incorporated into the SnO_2 matrix, the resistivity of the samples should undergo a considerable increase after the thermal treatment because (1) the correct stoichiometry of the SnO_2 crystal would be achieved and (2) re-evaporation of Sb atoms from the wires' surface. However, the resistivity remains unchanged after the thermal treatment ($\rho \simeq 4 \times 10^{-1}\Omega\,\mathrm{cm}$) and as a consequence, we believe that Sb doping was then effective [Fig. 3(b)].

Figure 4(a) displays the temperature dependent resistivity of a thin film built from a dispersion of wires, as described above, from 10 K to 300 K. The resistivity curve of undoped (0%) SnO_2 devices decreases as the temperature increases, as should be expected for semiconductors. This particular curve shows two distinct regions where Arrhenius-type [Fig. 4(b)] and variable range hopping mechanisms [Fig. 4(c)] were observed. The activation energy was extracted out from the high temperature range of the curve (90–300 K) using the slope of the semi-logarithmic plot of the resistivity as a function of reciprocal temperature. We found 50 meV for the activation energy in good agreement with literature data.[37,38] In the low temperature range (10–90 K), the electric transport is dominated by a hopping process. As mentioned above, vacancies not only provide carriers for the n-type character of the undoped SnO_2 but they are also a natural source of disorder that randomizes the local electronic potential leading to localization. The transport in these disordered systems is then characterized by

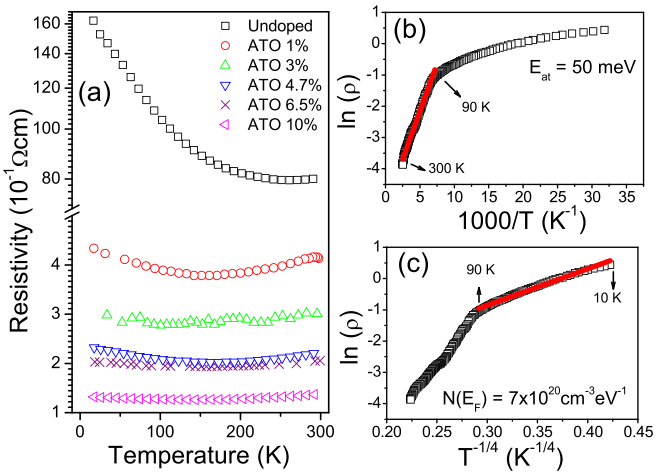

FIG. 4. Temperature dependent resistivity for thin film (built from a dispersion of wires) devices from 10 K to 300 K is plotted in panel (a). The undoped SnO_2 curves show a behaviour expected for semiconductors; the resistivity for doped devices was nearly temperature independent and lower than that observed in undoped devices. The analysis of the resistivity curve of the undoped thin film of wires has identified two distinct transport mechanisms: Arrhenius-type (panel b) and variable range hopping mechanisms (panel c). The red lines represent the fitting curves.

hopping between the localized states as pointed by Mott[39] and described by

$$\rho(T) = \rho_0 \exp\left[\left(\frac{T_0}{T}\right)^{\frac{1}{4}}\right], \tag{1}$$

where $T_0 = \frac{18\alpha^3}{k_B N(E_F)}$, $N(E_F)$ is the density of states at the Fermi level and α^{-1} is the localization length characterizing the spatial extension of wave functions. The conduction takes place by hopping of small region (k_BT) in the vicinity of the Fermi level where the density of states remains almost a constant. This condition is fulfilled when the temperature is sufficiently small or when the energy states are uniformly distributed. The agreement between theoretical and experimental curves confirms that the hopping process governs the transport from 10 to 90 K.[40] Fitting of Eq. (1) to the experimental data between 10 K and 90 K provides $N(E_F) = 7 \times 10^{20}\mathrm{cm}^{-3}\,\mathrm{eV}^{-1}$ when considering that $\alpha = (a_B)^{-1}$ where a_B is the Bohr radius of SnO_2 ($m^* = 0.24m_0$; $\varepsilon = 13.5$).[41,42] Additionally, the distance over which electrons hop was estimated to be $R_{hop} = 2.8$ nm at 300 K. The values obtained for the density of states and hopping distance are in agreement with the results observed by Serin *et al.* ($N(E_F) = 8.41 \times 10^{20}\mathrm{cm}^{-3}\,\mathrm{eV}^{-1}$, $R_{hop} = 1.99$ nm) in undoped SnO_2 thin films. Regardless of the structure of the samples, our results and those from Serin *et al.* point to the same behavior of the Sb doped SnO_2 structures.[22]

Careful inspection of resistivity curves of doped samples shows a transition from an insulating phase to a metallic one characterized by a diffusive transport exhibiting a weak dependence on the temperature (Fig. 5). Moreover, a careful inspection of these curves shows a singular shape: as seen in Fig. 5, the devices clearly undergo a transition from an insulating state ($dR/dT < 0$) to a metallic one ($dR/dT > 0$) around 130–150 K depending on the doping level. These

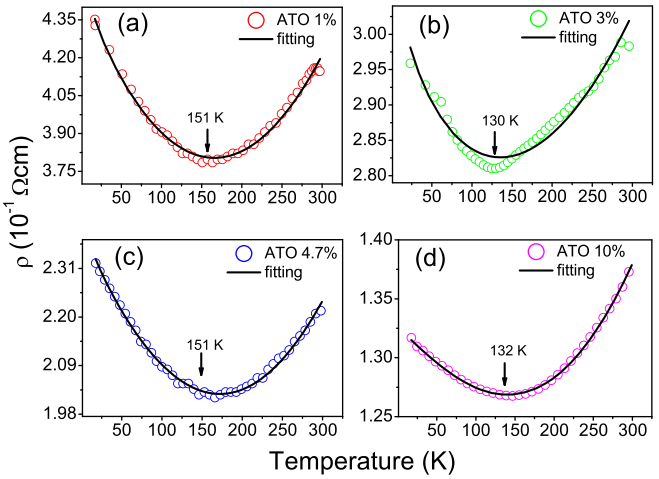

FIG. 5. Temperature dependent resistivity for four devices displaying a transition from an insulating to a metallic phase characterized by a diffusive transport exhibiting a weak dependence on the temperature. The data were successfully fitted to the weak localization and electron-electron interactions as displayed by the red lines. The devices clearly undergo a transition from an insulating state ($dR/dT < 0$) to a metallic one ($dR/dT > 0$) around 130 − 150 K depending on the doping level (as indicated by arrows).

changes on the temperature dependent resistivity are clear evidence of different scattering processes contributing to the electron transport in samples. At high temperatures ($T > 130$–150 K, depending on the doping level), the scattering processes are dominated by the electron-phonon interaction which randomizes the electron trajectories throughout the whole sample, producing the observed Drude-Boltzmann behaviour (metallic phase). The increase of the resistivity below 130 K seems not to be related to activation or hopping processes (as observed in undoped samples): successive attempts to distinguish an activation law or hopping behaviour have failed.

The minima observed in all resistivity curves indicate the transition between the two phases in the studied samples. When the mean free path becomes comparable to the Fermi wavelength ($k_F l \geq 1$) quantum corrections to the resistivity cannot be neglected (for our samples, $k_F l \simeq 1 - 3$): in this case, electron-electron interaction and weak localization corrections will determine the low temperature dependence of the conductivity of disordered metals and highly doped materials.[43] Assuming the Matthiessen rule for adding resistivities (in fact, to account for different scattering mechanisms), the resistivity can be written as

$$\rho(T) = \frac{1}{\sigma_0 + \Delta\sigma} + CT^2 = \frac{1}{\sigma_0 + AT^{3/2} + BT^{1/2}} + CT^2, \quad (2)$$

where $\Delta\sigma$ is the quantum correction to the conductivity described by $AT^{3/2}$ and $BT^{1/2}$, which account for weak localization and electron-electron contributions, respectively. In the absence of quantum corrections, the Boltzmann equation correctly describes the resistivity of the system: the term CT^2 represents the contribution of electron-electron scatterings in the low temperature range. The weak localization contribution is due to the self interference of backscattered wave functions and exponent 3/2 accounts for electron-phonon interactions. The sign of the B term depends on the characteristics of the system, such as inter-valley scattering, mass anisotropy, and level of disorder.[44]

Temperature dependent resistivity curves for samples with nominal Sb doping of 1, 3, 4.7, and 10% (Fig. 5) were analysed using Eq. (2). All parameters obtained from fitting are displayed in Table II.

Comparing the corrections to the conductivity from weak-localization and electron-electron interaction (A and B coefficients, respectively) one can notice that the contribution of the electron-electron interactions is more pronounced. It should be expected that with increasing disorder the intensity of electron-electron interactions will be enhanced. However, data in Table II show a weak variation of B values, and taking into account that the $k_F l$ term remains almost unchanged for all samples, these results point to almost the same level of the disorder for different samples. This observation agrees with LIBS and Hall data showing that the sample structure (and consequently the disorder level) is not highly affected by the doping [Fig. 2]. Regarding the temperature range used in experiments, other scattering mechanisms such as electron-phonon interactions should affect the results.

In order to investigate the presence of the electron-phonon interactions in our samples, we conducted some fittings based on simple assumptions. Following the paper from Leo and Ramakrishnan,[44] the expression $\rho(T) = \rho_0 + CT^n$ holds for metals in the low temperature regime where Bloch waves are scattered by impurities. Increasing the temperature, phonons are excited and both scattering events (impurities and phonons) and the exponent n increase ($n > 2$). At high temperatures (those above minima in curves of Fig. 5), the electron-acoustic phonon scattering mechanism begins to contribute to the transport properties and the resistivity (metal-like) can be correctly described by the Bloch-Grü neisen equation[45]

$$\rho(T) = \rho_0 + \left(\frac{T}{\Theta_D}\right)^q \int_0^{\frac{\Theta_D}{T}} \frac{z^q e^z}{(e^z - 1)^2} dz, \quad (3)$$

where ρ_0 is a constant and q usually ranges from 3 to 5 when the electron-phonon interaction is mainly responsible for the scattering events;[43,45] Θ_D is the Debye temperature. As the temperature and phonon excitations increase, the amount of scattering events experienced by the conduction electrons is increased as well, resulting in a greater resistivity. In fact, as the Debye temperature of SnO_2 is approximately 500–600 K,[46,47] Eq. (3) can be simplified to

TABLE II. Best fitting parameters for Eq. (2).

Doping level → *parameters* [Eq. (2)]↓	1%	3%	4.7%	10%
$\sigma_0(\pm 2)$	215	304	405	751
$A(\pm 0.01)$	0.02	0.001	0.04	0.04
$B(\pm 0.1)$	3.2	6.2	4.9	1.4
$C(\pm 0.5 \times 10^{-9})$	1.7×10^{-9}	1.5×10^{-9}	9.6×10^{-9}	4.0×10^{-9}

$$\rho(T) \simeq \rho_0 + A\left(\frac{T}{\Theta_D}\right)^5. \quad (4)$$

Using Eq. (3) or Eq. (4) for fitting the high temperature range of resistivity curves in Fig. 5, we found for all samples $\Theta_D = (615 \pm 8)$K in full agreement with the tabled Debye temperature of SnO_2.[46,47] The Bloch–Grüneisen law (T^5-law) is a characteristic of crystalline materials showing that long wavelength lattice waves can travel in a perfect crystal at low temperatures ($T < \Theta_D$). Indirectly, this confirms the good crystalline character of our samples in agreement with the X-ray analysis.

From the above data, we observed a metal to insulator transition associated with the Sb doping. All samples have been characterized by doping levels near or above the Mott limit $n_c = 6.7 \times 10^{17}\text{cm}^{-3}$ [see Fig. 2], thus fulfilling the Mott criterion for MIT observation. The increase of the resistivity at low temperatures is thus a consequence of the enhancement of the electron-electron interaction while at the high temperature limit, electron-phonon interactions dominate the transport processes.

V. CONCLUSION

In summary, crystalline Sb doped SnO_2 wires were grown from chemical vapour deposition. We do not find significant changes in the lattice parameters as a function of the increasing doping level meaning that the Sb doping seems not to strongly affect the structure of the SnO_2. Comparing LIBS and Hall data and the resistivity response, it is clear that the disorder level is not highly affected by the doping as experimentally observed. The increase of the doping level led to a clear transition from a semiconductor to a metallic behaviour, as well as a reasonable correspondence between the resistivity and the incorporated dopant concentration was observed. We identified hopping and activation electron transport mechanisms in undoped samples (insulating phase), whereas after doping, the electron-electron mechanism appeared to be the dominant scattering process. Also, in the high temperature range, electron-phonon scattering was observed leading to the calculation of the Debye temperature for the samples in good agreement with the literature.

ACKNOWLEDGMENTS

The authors thank the financial support from the Brazilian agencies: Grant Nos. 2013/19692-0, São Paulo Research Foundation (FAPESP) and Grant Nos. 302640/2010-0 and 305615/2014-9 (CNPq).

[1]J. Robertson, Phys. Rev. B **30**, 3520 (1984).
[2]S. Luo, J. Fan, W. Liu, M. Zhang, Z. Song, C. Lin, X. Wu, and P. K. Chu, Nanotechnology **17**, 1695 (2006).
[3]Z. R. Dai, J. L. Gole, J. D. Stout, and Z. L. Wang, J. Phys. Chem. B **106**, 1274 (2002).
[4]J. G. Lu, P. Chang, and Z. Fan, Mater. Sci. Eng. R **52**, 49 (2006).
[5]Q. Wan and T. H. Wang, Chem. Commun. **30**, 3841 (2005).
[6]A. Kolmakov, D. O. Klenov, Y. Lilach, S. Stemmer, and M. Moskovits, Nano Lett. **5**, 667 (2005).
[7]M. Lei, Q. R. Hu, S. L. Wang, and W. H. Tang, Mater. Lett. **64**, 19 (2010).
[8]Y. Shen, T. Yamazaki, Z. Liu, D. Meng, and T. Kikuta, J. Alloys Compd. **488**, L21 (2009).
[9]Y.-H. Lin, Y.-C. Hsueh, P.-S. Lee, C.-C. Wang, J. M. Wu, T.-P. Perng, and H. C. Shih, J. Mater. Chem. **21**, 10552 (2011).
[10]L. Liu, T. Zhang, L. Wang, and S. Li, Mater. Lett. **63**, 2041 (2009).
[11]M. Herrera, D. Maestre, A. Cremades, and J. Piqueras, J. Phys. Chem. C **117**, 8997 (2013).
[12]Z. Wang and L. Liu, Mater. Lett. **63**, 917 (2009).
[13]C. A. Amorim, C. J. Dalmaschio, E. R. Leite, and A. J. Chiquito, J. Phys. D: Appl. Phys. **47**, 045301 (2013).
[14]C. A. Amorim, C. J. Dalmaschio, A. L. R. Melzi, E. R. Leite, and A. J. Chiquito, J. Phys. Chem. Solids **75**, 583 (2014).
[15]H. T. Feng, R. F. Zhuo, J. T. Chen, D. Yan, J. J. Feng, H. J. Li, S. Cheng, and P. X. Yan, Physica E **41**, 1640 (2009).
[16]M. E. White, O. Bierwagen, M. Y. Tsai, and J. S. Speck, J. Appl. Phys. **106**, 93704 (2009).
[17]S. V. Eremeev, O. I. Velikokhatnyi, P. N. Kumta, and A. I. Potekaev, Russ. Phys. J. **47**, 701 (2004).
[18]P.-S. Lee, Y.-H. Lin, Y.-S. Chang, J.-M. Wu, and H. C. Shih, Thin Solid Films **519**, 1749 (2010).
[19]Q. Wan, E. N. Dattoli, and W. Lu, Appl. Phys. Lett. **90**, 222107 (2007).
[20]Z. Q. Li, Y. L. Yin, X. D. Liu, L. Y. Li, H. Liu, and Q. G. Song, J. Appl. Phys. **106**, 083701 (2009).
[21]C. Ke, W. Zhu, Z. Zhang, E. S. Tok, B. Ling, and J. Pan, Sci. Rep. **5**, 17424 (2015).
[22]T. Serin, A. Yildiz, N. Serin, N. Yildirim, F. Özyurt, and M. Kasap, J. Electron. Mater. **39**, 1152 (2010).
[23]P. W. Anderson, Phys. Rev. **109**, 1492 (1958).
[24]B. I. Shklovskii and A. L. Efros, *Electronic Properties of Doped Semiconductors* (Springer Verlag, Berlin, 1984).
[25]L. van der Pauw, Philips Res. Rep. **13**, 1 (1958).
[26]S.-Y. Lee and B.-O. Park, Thin Solid Films **510**, 154 (2006).
[27]H. M. Rietveld, J. Appl. Crystallogr. **2**, 65 (1969).
[28]R. A. Young, *The Rietveld Method* (Oxford University Press, New York, 1993).
[29]A. C. Larson and R. B. Von Dreele, *GSAS General Structure Analysis System* (Los Alamos National Laboratory, Los Alamos, 2004).
[30]B. H. Toby, J. Appl. Crystallogr. **34**, 210 (2001).
[31]B. Thangaraju, Thin Solid Films **402**, 71 (2002).
[32]A. A. Zhukova, M. N. Rumyantseva, A. M. Abakumov, J. Arbiol, L. Calvo, and A. M. Gaskov, Thin Solid Films **518**, 1359 (2009).
[33]N. Naghavi, C. Marcel, L. Dupont, J. B. Leriche, and J. M. Tarascon, Solid State Ionics **156**, 463 (2003).
[34]R. D. Shannon, Acta Crystallogr. Sect. A **32**, 751 (1976).
[35]N. Keshava, IEEE Trans. Geosci. Remote Sens. **42**, 1552 (2004).
[36]B. S. Marangoni, K. S. G. Silva, G. Nicolodelli, G. S. Senesi, J. S. Cabral, P. R. Villas-Boas, C. S. Silva, P. C. Teixeira, A. R. A. Nogueira, V. M. Benites *et al.*, Anal. Methods **8**, 78 (2016).
[37]E. Viana, J. González, G. Ribeiro, and A. de Oliveira, Phys. Status Solidi RRL **6**, 262 (2012).
[38]C. Fonstad and R. Rediker, J. Appl. Phys. **42**, 2911 (1971).
[39]N. F. Mott, *Metal-Insulator Transitions* (Taylor and Francis, London, 1990).
[40]E. Viana, J. González, G. Ribeiro, and A. De Oliveira, J. Phys. Chem. C **117**, 7844 (2013).
[41]K. J. Button, C. G. Fonstad, and W. Dreybrodt, Phys. Rev. B **4**, 4539 (1971).
[42]H. Hosono, D. C. Paine, and D. Ginley, *Handbook of Transparent Conductors* (Springer Science and Business Media, 2010).
[43]B. L. Altshuler and A. G. Aronov, *Electron-Electron Interactions in Disordered Systems*, edited by A. L. Efros and M. Pollak (North-Holland, Amsterdam, 1985).
[44]P. A. Lee and T. V. Ramakrishnan, Rev. Mod. Phys. **57**, 287 (1985).
[45]J. M. Ziman, *Electrons and Phonons: The Theory of Transport Phenomena in Solids* (Oxford University Press, London, 1960).
[46]K. J. Bachmann, F. S. L. Hsu, and J. P. Remeika, Phys. Status Solidi **67**, K39 (1981).
[47]P. Turkes, C. Pluntke, and R. Helbig, J. Phys. C: Solid State Phys. **13**, 4941 (1980).